applied sciences

MDPI

Article

Pairing Hamiltonians of Nearest-Neighbour-Interacting Superconducting Qubits on IBM Quantum Computer

Shirshendu Chatterjee [1], Bikash K. Behera[2] and Felix J. Seo[3,*]

[1] Department of Electrical and Computer Engineering, University of California Santa Barbara, Santa Barbara, CA 93106, USA; shirshendu@ucsb.edu
[2] Bikash's Quantum (OPC) Pvt. Ltd., Balindi, Mohanpur 741246, West Bengal, India; bikas.riki@gmail.com
[3] Department of Physics, Hampton University, Hampton, Virginia, 23668, USA; jaetae.seo@hamptonu.edu
* Correspondence : jaetae.seo@hamptonu.edu

Abstract: Quantum Simulation experiment of pairing Hamiltonians of nearest-neighbour interacting superconducting qubits was performed with a complete set of algorithms in an IBM Quantum Computer- IBMq Lima. The experiment revealed the fidelity as a function of iteration using Suzuki-Trotter decomposition for four different types of nearest-neighbour Heisenberg, XY, transverse, and longitudinal Ising superconducting qubit couplings of Hamiltonians. The experiment displayed the models how the experimental density matrices shift from the theoretical density matrices and also their behavior with number of iterations. It also proved the reconstruction of quantum states and how the states change as function of iteration with the IBM Quantum Computer- IBMq Lima. Along with that the time evolution of the states for different models were also seen to predict the dominance of each state.

Keywords: Quantum Simulation Experiment, Coupling Hamiltonians of superconducting qubits, Fidelity vs. Iteration

1. Introduction

A simulation of many-body quantum-mechanical dynamics is not a simple computational problem due to the exponential growth of complexity [1]. A quantum simulation was proposed to solve such an exponential explosion problem using a controllable quantum system in early 1980 [2]. It was shown in 1996 [3] that a quantum computer only containing few particle interactions can be used to efficiently simulate the many-body quantum Hamiltonians [4]. The quantum computation has recently simulated the various dynamics in condensed- matter physics, high-energy physics [5], quantum chemistry, physics [6], high quantum information processing [7] and quantum gravity [8] using a quantum computer with superconducting qubits. In addition, several number of qubit systems including neutral atoms [9], ions [10], polar molecules [11], electrons or nuclear spins in semiconductors quantum dots [12] and photons [13] have been proposed for the quantum simulating systems. Among the qubit systems, the trapped ion qubits [14] and photons qubits [13] have already been experimentally demonstrated to some extent.

Since Benioff proposed a microscopic quantum mechanical model of computers with Turning machines proposed in 1979, and Feynman conjectured that quantum computer can be programmed to simulate any local quantum system [28], the development of quantum computer and quantum system has been continued over the past three decades [18, 19]. The quantum computer has high computational power with a small number of qubits.

Citation: To be added by editorial staff during production.

Academic Editor: Firstname Lastname

Received: date
Revised: date
Accepted: date
Published: date

The quantum simulation recently has been of great interest because of high computational power, less energy consumption, and exponential speed over classic computer for the quantum many-body systems in physics [15], chemistry [20] and even biology [21]. A great number research groups are now actively focusing at the experimental realization of quantum simulators with tens of qubits, which would be the first practical applications in which quantum computers outperform their classical counterparts [17].

Pairing Hamiltonians, e.g., BCS Hamiltonian [22] in the type-1 superconductors feature long-range many- body interactions which are generally intractable on classical computers. Nevertheless, large-scale numerical calculations based on pairing Hamiltonians are of great im- portance, in superconducting quantum computer technology in addition to the scientific studies of quantum systems of mesoscopic condensed matter, ultrasmall metallic grains and heavy nuclei [23]. To tackle this problem, a polynomial time quantum algorithm based on a nuclear magnetic resonance (NMR) [24] quantum computer was proposed, however liquid NMR has several constrains- that make NMR quantum computer not scalable. Thus, large-scale implementation of the NMR- based quantum algorithm is unlikely in conformity with the state-of-the-art technology [24].

Superconducting quantum circuits [25] have rapidly progressed in the past decades, thus enabling them to be one of the most promising candidates towards practical quantum information processing. The flexible design and fabrication, the affordable various Hamiltonians and the mature technology also allow to scale up the superconducting quantum computer. Moreover, the research on other solid-state qubit devices, e.g., quantum dot in semiconductors [26] and defect systems have also made significant progress in the past years. In the past few decades, the awareness has grown in the scientific world that the quantum computation may be a more natural and desirable method of computation than the classical one. The visible difficulty of solving a problem of quantum many-body physics of fermions (and bosons) on a classical computer demands an exponentially large basis set [27]. Lloyd proposed the first technologically feasible design for a quantum computer [28]. The advancement of quantum computing technology has been continued and many quantum algorithms are also available for the practical applications in simulating, computing, factoring and featuring. Recently, the IBM Q has provided a platform to simulate many quantum problems using the quantum circuits with operational gates and algorithms [29,30]. Utilizing the IBM Q Experience platform, a large number of experiments have been performed for the quantum information, quantum simulation [39-43], quantum key distribution [44], quantum teleportation [45], quantum cryptography [46,47], quantum currency [48], quantum devices [49,50] etc.

In this article, four different pairing Hamiltonians of nearest-neighbor-interacting superconducting qubits are simulated a set of complete algorithms which are suitable for a wide range of models especially superconducting and semiconducting qubit systems. The quantum state tomography has been computed and calculated the fidelity as a function of iterations using the Suzuki-Trotter decomposition for 2 qubits system. The time evolution of the system by tuning interaction parameters have been studied.

2. Model

2.1 Pairing Hamiltonian in Superconductivity

The BCS pairing Hamiltonian has been widely used in different fields of physics- condensed matter physics, nuclear physics etc. The Hamiltonian is typically expressed in terms of bosonic or fermionic creation (annihilation) operators- - $\mathbf{c}^{\dagger}_{\pm\mathbf{m}}$and $\mathbf{c}_{\pm\mathbf{l}}$ and $\mathbf{n}^{\mathbf{F}}_{\pm\mathbf{l}} = \mathbf{c}^{\dagger}_{\pm\mathbf{m}}\mathbf{c}_{\pm\mathbf{m}}$are fermionic number operators.

$$H_{BCS} = \sum_{m=1}^{N} \frac{\epsilon_m}{2} (n_m^F + n_{-m}^F) + \sum_{l=1}^{N} \sum_{m=1}^{N} V_{ml}\, c_m^\dagger c_{-m}^\dagger c_{-l} c_l \quad (1)$$

where, the matrix elements are real and can be estimated or calculated, e.g., for superconductors, in terms of Coulomb force and the electron phonon interaction. Pairs of fermions are labeled by the quantum numbers m and -m, according to the Cooper pair situation where paired electrons have equal energies but opposite momenta and spins: m = (p, ↑) and -m = (-p, ↓). This is seen in Fig 1. These are time-reversed and degenerate partners whose energies are considered to be phenomenological parameters. In order to realize the quantum simulation, the BCS Hamiltonian is transformed to the Hamiltonian with Pauli operators which can be mapped on a system of qubits with the algebraic morphism between spins and fermions.

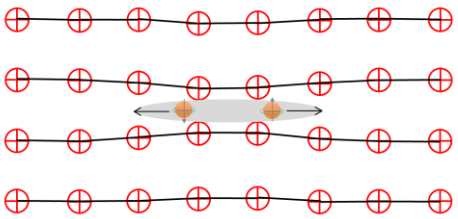

Figure 1. Pictorial representation of the BCS Pairing Theory.

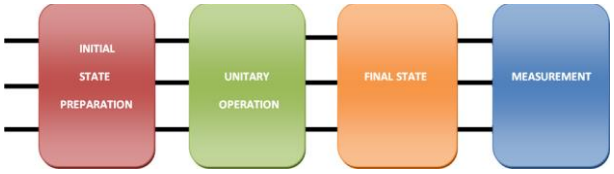

Figure 2. Schematic diagram of the method of simulation of the 2-qubits pairing Hamiltonian.

Then, the fermionic pair operators can be mapped onto a system of qubits which can be represented by the Pauli operators of σ_m^x, σ_m^y, σ_m^z through transformation $\{\sigma_m^x, \sigma_m^y, \sigma_m^z\} = \{c_m^\dagger c_{-m}^\dagger + c_{-m} c_m,\ ic_{-m} c_m + ic_m^\dagger c_{-m}^\dagger,\ n_m^F + n_{-m}^F - 1\}$.

The transformed Hamiltonian from Eq.(1) can be re-written in the qubit form as-

$$H_{BCS} = \sum_{m=1}^{N} \frac{\epsilon_m}{2} \sigma_m^z + \sum_{m<l} \frac{V_m}{2} \left(\sigma_m^x \sigma_l^x + \sigma_m^y \sigma_l^y\right) \quad (2)$$

where, $\varepsilon_m = \epsilon_m + V_{mm}$

Table 1. Interaction Hamiltonians

Interaction Models	Interaction Hamiltonians
Heisenberg Model	$H_H = H_0 + \sum_{i=x,y,z} \sum_{l=1}^{N-1} J_l^i \sigma_l^i \sigma_{l+1}^i$
XY Model	$H_{XY} = H_0 + \sum_{i=x,y} \sum_{l=1}^{N-1} J_l^i \sigma_l^i \sigma_{l+1}^i$
Transverse Ising Model	$H_{TIsing} = H_0 + \sum_{l=1}^{N-1} J_l \sigma_l^x \sigma_{l+1}^x$
Longitudinal Ising Model	$H_{LIsing} = H_0 + \sum_{l=1}^{N-1} J_l \sigma_l^z \sigma_{l+1}^z$

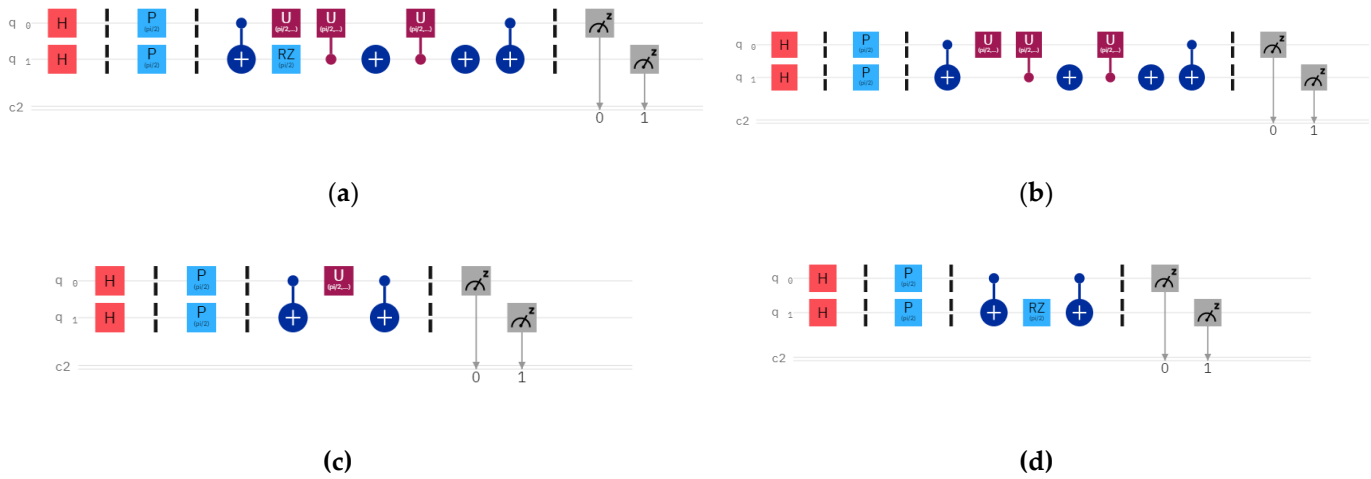

Figure 3. Quantum circuits for the nearest-neighbour-interacting (a) Heisenberg (b) XY (c) transverse Ising (d) longitudinal Ising Hamiltonian models.

2.2. Nearest-Neighbour Coupling Interactions in Superconductivity

The coupling of qubits can be achieved through various type of interactions. For superconducting qubits, the coupling can be done through many ways such as through inductance, capacitance or Josephson junctions. The interaction models can be classified into four categories- XY, Heisenberg, transverse Ising and longitudinal Ising. These four types of Hamiltonians can be written together as-

$$\boldsymbol{H = H_0 + H_I} \quad (3)$$

$\boldsymbol{H_0}$ is the single qubit Hamiltonian.

$$\boldsymbol{H_0 = \sum_{l=1}^{N} \frac{1}{2} \omega_l \sigma_l^z} \quad (4)$$

and $\boldsymbol{H_I}$ denoting the interaction Hamiltonian,

$$\boldsymbol{H_I = \sum_{l=1}^{N-1} \left(J_l^x \sigma_l^x \sigma_{l+1}^x + J_l^y \sigma_l^y \sigma_{l+1}^y + J_l^z \sigma_l^z \sigma_{l+1}^z \right)} \quad (5)$$

Here $\boldsymbol{\sigma_l^x, \sigma_l^y, \sigma_l^z}$ are the Pauli matrices in the basic of $\boldsymbol{\sigma_l^z}$ and l denotes the $\boldsymbol{l^{th}}$qubit. The coupling strength between the $\boldsymbol{l^{th}}$and the $\boldsymbol{l + 1^{th}}$qubits is denoted by $\boldsymbol{J_{l,l+1}}$ (l=1,...,N-1). The parameters of the previous two equations are chosen to get the Hamiltonian of four different models and $\boldsymbol{J_l}$ is fixed accordingly. It can be seen that the pairing models in Eq. 2 does not follow the form of the Hamiltonians of Eq. 3. Thus, it is imperative to design algorithms to simulate these pairing Hamiltonians using the four types of interaction Hamiltonian. For the operators $\boldsymbol{\sigma_m^x, \sigma_m^y, \sigma_m^z}$ it should be taken care when simulating in the Suzuki-Trotter decomposition as the operators may not commute. It is noted that the tunability of parameters $\boldsymbol{\omega_l (l = 1, \ldots, N)}$ and $\boldsymbol{J_l^i (i = x, y, z, l = 1, \ldots, N - 1)}$ affects the efficiency of the algorithms.

3. Methods of Simulation for Hamiltonian Operator

The method of simulating the Hamiltonians for each model is shown in Fig 2., where the initial state of the qubits is prepared then the final state is prepared after the unitary

operator works on the final state and then doing the measurement and mapping to the classical register.

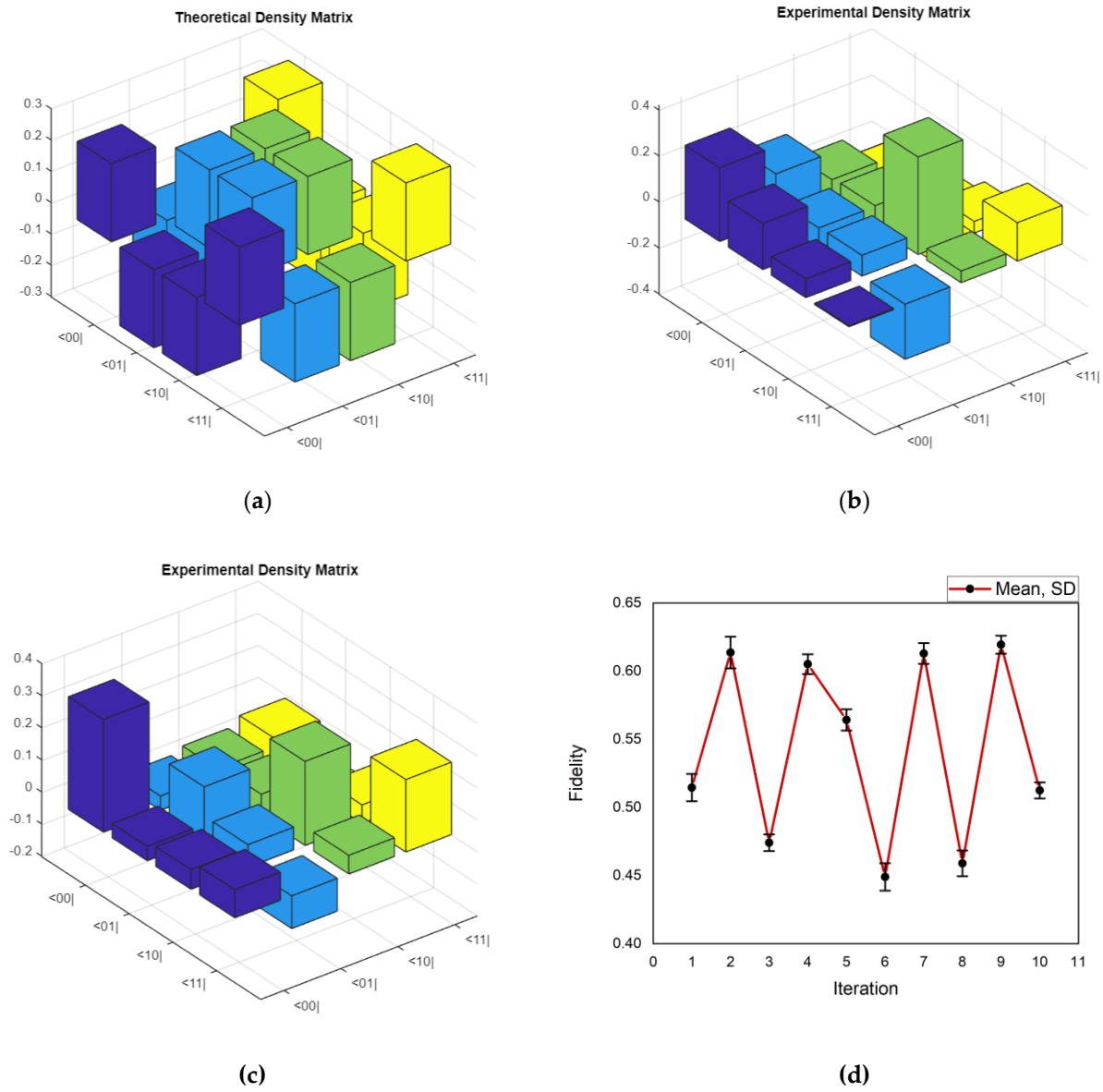

Figure 4. (a) Theoretical density matrix for the Heisenberg model, (b) Experimental density matrix for 2 iterations, (c) Experimental density matrix for 10 iterations, (d) Fidelity as a function of iteration.

Given the initial state at the time $t = 0$, it can be solved it to obtain the state at any later instant [55]. If $\hat{H}$ is independent of time, then

$$|\psi(x,t)\rangle = e^{-i\hat{H}t}|\psi(0)\rangle \quad (6)$$

where, $U(t) = e^{-i\hat{H}t}$ is the time evolution operator. $U(t)$ is a unitary operator, i.e., $U^{\dagger}U = I$. For our case, simulation of four different Hamiltonian was done thus finding the corresponding unitary operations to build the quantum circuit.

In general, to find the matrices for the time evolution operator it is to be seen how the terms $\widehat{\sigma^x}$, $\widehat{\sigma^y}$, $\widehat{\sigma^z}$, $\widehat{\sigma^x}\widehat{\sigma^x}$, $\widehat{\sigma^y}\widehat{\sigma^y}$, $\widehat{\sigma^z}\widehat{\sigma^z}$ look like. Then the terms can be separated for x, y, z as $\widehat{\sigma^x}\widehat{\sigma^x}$, $\widehat{\sigma^y}\widehat{\sigma^y}$, and $\widehat{\sigma^z}\widehat{\sigma^z}$ commute with each other. The Hamiltonian of our choice is-

$$H = \sum_{l=1}^{N} \frac{1}{2}\omega_l \sigma_l^z + \sum_{l=1}^{N-1}\left(J_l^x \sigma_l^x \sigma_{l+1}^x + J_l^y \sigma_l^y \sigma_{l+1}^y + J_l^z \sigma_l^z \sigma_{l+1}^z\right) \quad (7)$$

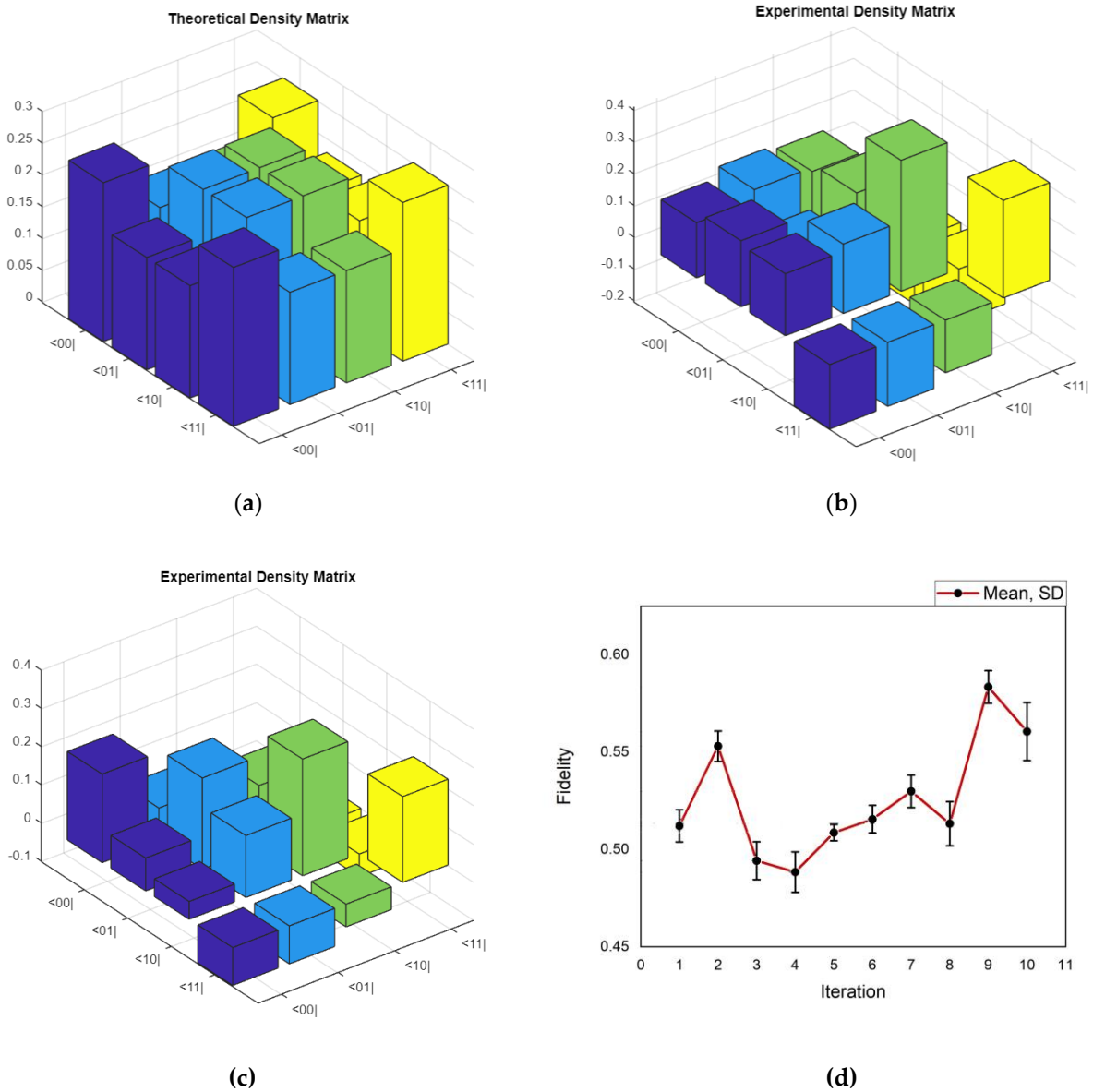

Figure 5. (a) Theoretical density matrix for the XY model, (b) Experimental density matrix for 2 iterations, (c) Experimental density matrix for 10 iterations, (d) Fidelity as a function of iteration.

The corresponding time evolution operator is given by-

$$U(t) = e^{-i\left(\sum_{l=1}^{N}\frac{1}{2}\omega_l\sigma_l^z\right)t} e^{-i\sum_{l=1}^{N-1}\left(J_l^x\sigma_l^x\sigma_{l+1}^x + J_l^y\sigma_l^y\sigma_{l+1}^y + J_l^z\sigma_l^z\sigma_{l+1}^z\right)t} \quad (8)$$

Here $\widehat{\sigma^x} = \begin{bmatrix} 0 & 1 \\ 1 & 0 \end{bmatrix}$, $\widehat{\sigma^y} = \begin{bmatrix} 0 & -i \\ i & 0 \end{bmatrix}$, $\widehat{\sigma^z} = \begin{bmatrix} 0 & -i \\ i & 0 \end{bmatrix}$

The first part of the operator can be written as per the value of Pauli matrix $\widehat{\sigma^z}$ shown. The term $e^{-iJ_l\widehat{\sigma^x}\widehat{\sigma^x}t}$ in the second part of the operator can be written as,

$$I\cos J_l t - \widehat{\sigma^x} \otimes \widehat{\sigma^x} i\sin J_l t = \begin{bmatrix} \cos(J_l t) & 0 & 0 & -i\sin(J_l t) \\ 0 & \cos(J_l t) & -i\sin(J_l t) & 0 \\ 0 & -i\sin(J_l t) & \cos(J_l t) & 0 \\ -i\sin(J_l t) & 0 & 0 & \cos(J_l t) \end{bmatrix} \quad (9)$$

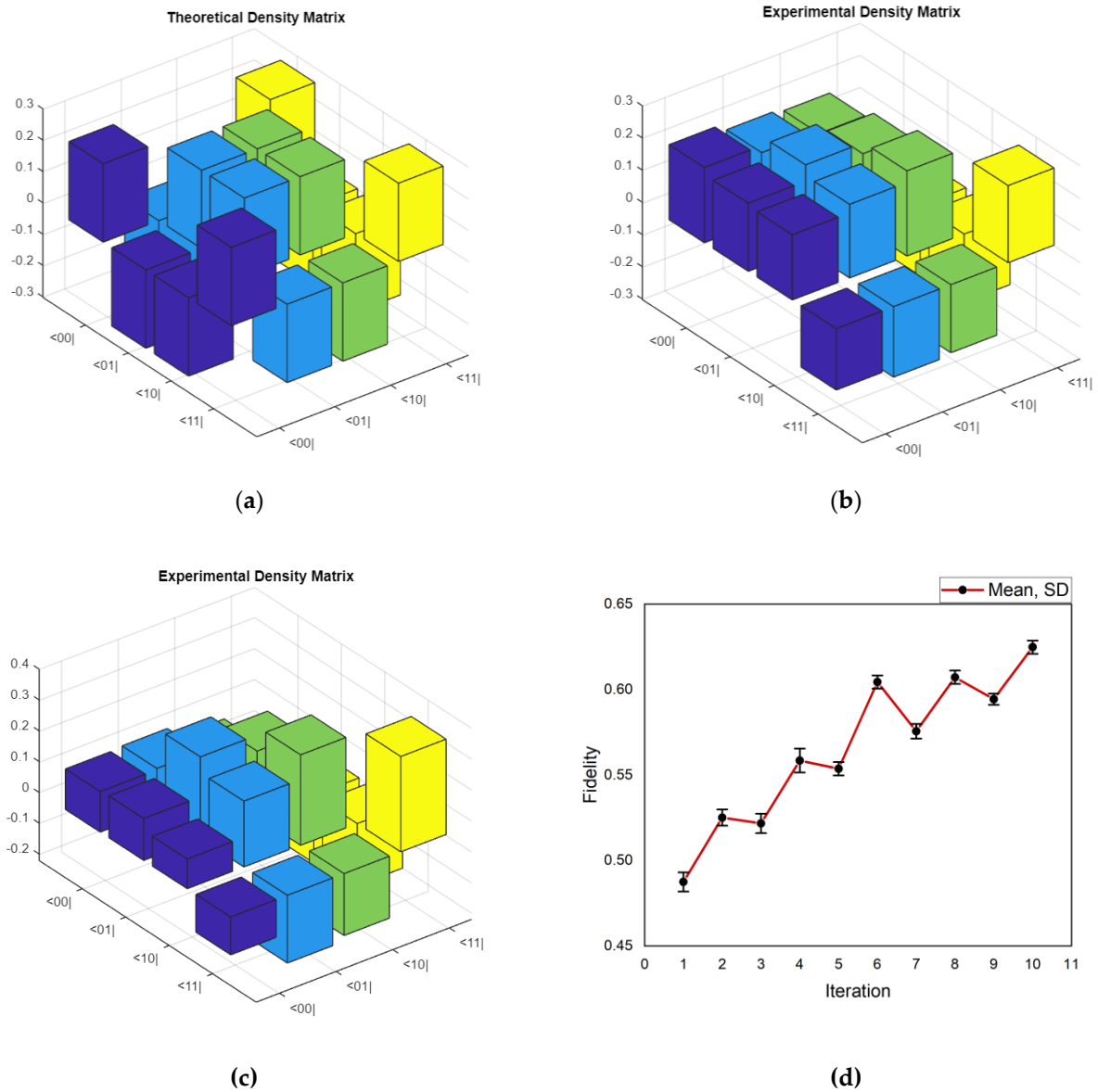

Figure 6. (a) Theoretical density matrix for transverse Ising model, (b) Experimental density matrix for 2 iterations, (c) Experimental density matrix for 10 iterations, (d) Fidelity as a function of iteration.

The term $e^{-iJ_l\widehat{\sigma^y}\widehat{\sigma^y}t}$ in the second part of the operator can be written as,

$$Icos\,J_lt - \widehat{\sigma^y} \otimes \widehat{\sigma^y} isin\ J_lt = \begin{bmatrix} \cos(J_l t) & 0 & 0 & i\sin(J_l t) \\ 0 & \cos(J_l t) & -i\sin(J_l t) & 0 \\ 0 & -i\sin(J_l t) & \cos(J_l t) & 0 \\ i\sin(J_l t) & 0 & 0 & \cos(J_l t) \end{bmatrix} \quad (10)$$

The term $e^{-iJ_l\widehat{\sigma^y}\widehat{\sigma^y}t}$ in the second part of the operator can be written as,

$$Icos\,J_lt - \widehat{\sigma^y} \otimes \widehat{\sigma^y} isin\ J_lt = \begin{bmatrix} e^{-J_l t} & 0 & 0 & 0 \\ 0 & e^{J_l t} & 0 & 0 \\ 0 & 0 & e^{J_l t} & 0 \\ 0 & 0 & 0 & e^{-J_l t} \end{bmatrix} \quad (11)$$

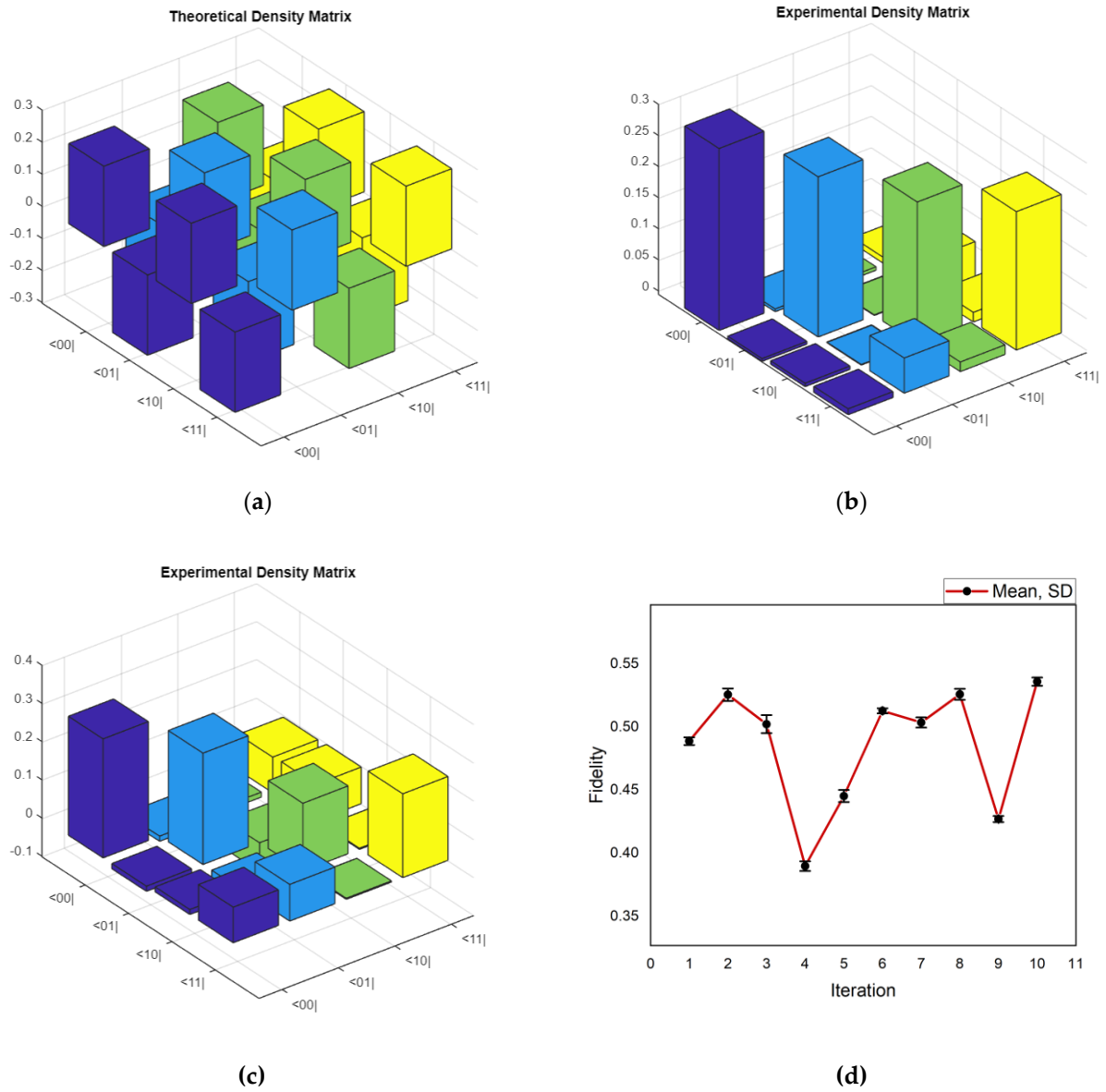

Figure 7. (a) Theoretical density matrix for longitudinal Ising Model, (b) Experimental density matrix for 2 iterations, (c) Experimental density matrix for 10 iterations, (d) Fidelity as a function of iteration.

Now, referring to the four Hamiltonian's, the time evaluation operator can be written and thus proceed to implementation. Each of these four types of Hamiltonians is a special case of Eq. 7 with parameters being properly chosen. The Hamiltonian can be thus reduced to the (i) longitudinal Ising Hamiltonian for parameters $J_l^x = J_l^y = 0$ and $J_l^z = J_l$; (ii) transverse Ising Hamiltonian for parameters $J_l^y = J_l^z = 0$ and $J_l^x = J_l$; (iii) XY Hamiltonian for parameters $J_l^z = 0$ and $J_l^x = J_l^y = J_l$; (iv) Heisenberg Hamiltonian for parameters $J_l^x = J_l^y = J_l^z = J_l$.

The following step is to implement the unitary operator in a quantum circuit as obtained from the previous calculations. So, elaborating the whole calculation-

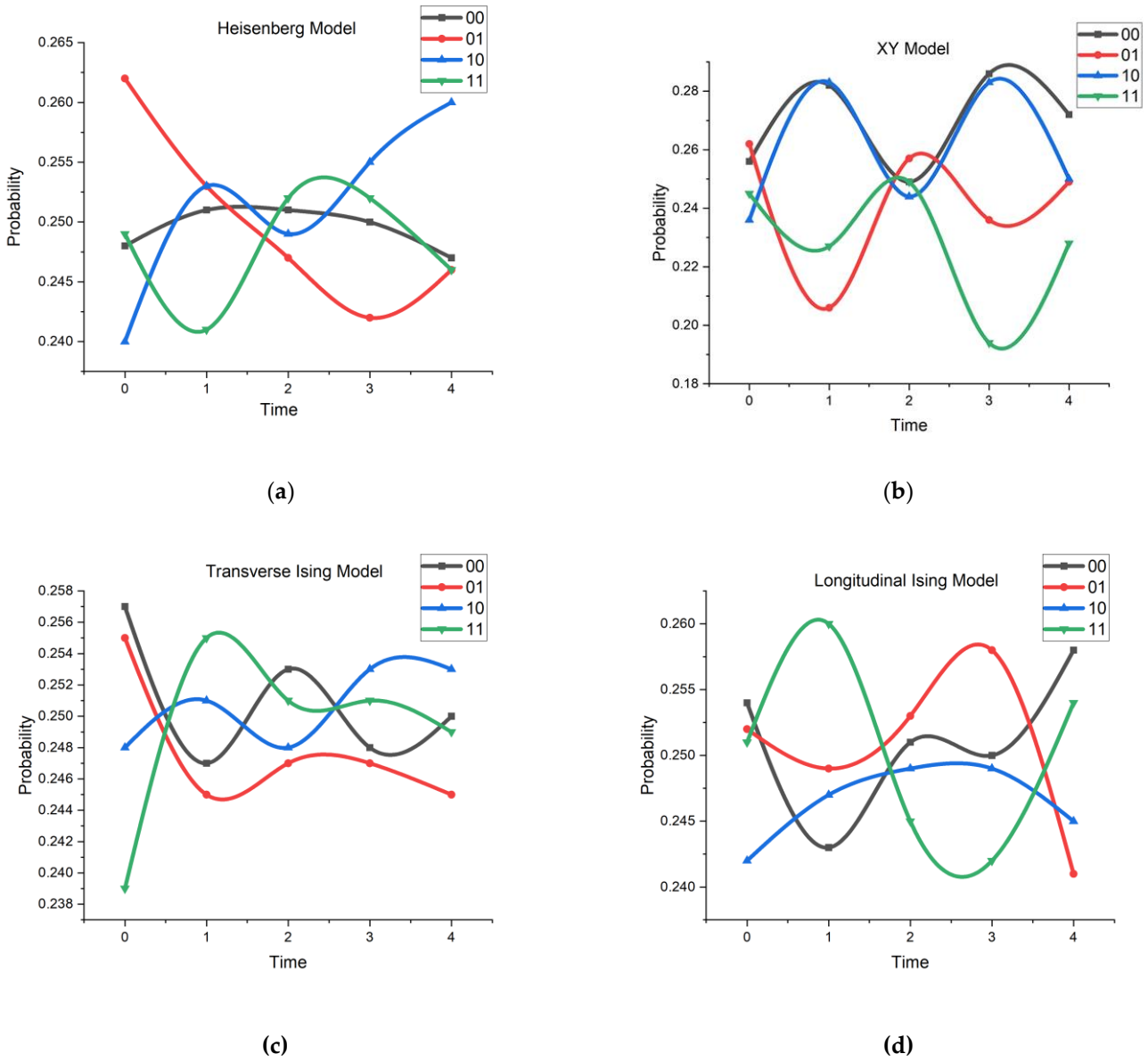

Figure 8. (a) Time Evolution of different Models at $\frac{\theta}{2}$ for (a)Heisenberg, (b) XY, (c) transverse Ising, and (d) longitudinal Ising model.

In General

The Hamiltonian is given by-

$$H = \sum_{l=1}^{N} \frac{1}{2}\omega_l \sigma_l^z + \sum_{l=1}^{N-1}\left(J_l^x \sigma_l^x \sigma_{l+1}^x + J_l^y \sigma_l^y \sigma_{l+1}^y + J_l^z \sigma_l^z \sigma_{l+1}^z\right) \quad (12)$$

which is simplified for a 2-qubit system:

$$H = \frac{1}{2}\omega_1 \sigma_1^z + \frac{1}{2}\omega_1 \sigma_2^z + \left(J_1^x \sigma_1^x \sigma_2^x + J_1^y \sigma_1^y \sigma_2^y + J_1^z \sigma_1^z \sigma_2^z\right) \quad (13)$$

For XX operation:

The term $\widehat{\sigma^x}\widehat{\sigma^x}$ of the Hamiltonian is to be decomposed to form the circuit.

Let us consider the *U3* gate

$$U3(\theta, \phi, \lambda) = \begin{bmatrix} \cos\theta/2 & e^{-i\lambda}\sin\theta/2 \\ e^{i\phi}\sin\theta/2 & e^{i(\phi+\lambda)}\cos\theta/2 \end{bmatrix}$$

$$U3\left(\theta, \phi = -\frac{\pi}{2}, \lambda = \frac{\pi}{2}\right) = \begin{bmatrix} \cos\theta/2 & -i\sin\theta/2 \\ -i\sin\theta/2 & \cos\theta/2 \end{bmatrix} \quad (14)$$

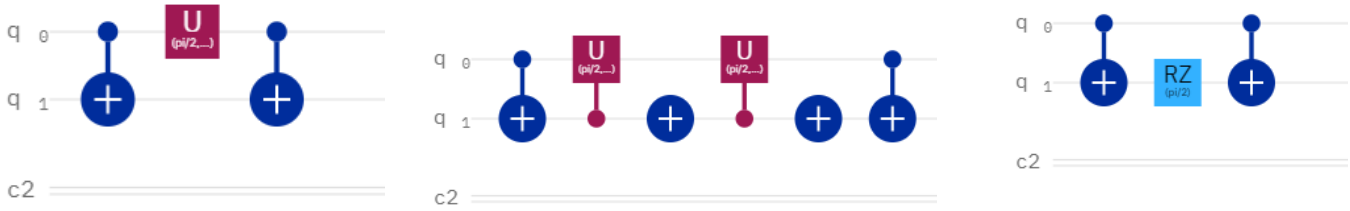

(**a**) (**b**) (**c**)

Figure 9. (a) Circuit Implementation for the different interaction of (a) $\widehat{\sigma_1^x}\widehat{\sigma_2^x}$ term the circuit consists of two CNOT gates and one U3 gate, (b) $\widehat{\sigma_1^y}\widehat{\sigma_2^y}$ term the circuit consists of two CNOT gates and one U3 gate, one $U3^\dagger$ gate and two NOT gates, and (c) $\widehat{\sigma_1^z}\widehat{\sigma_2^z}$ term the circuit consists of two CNOT gates and one Rz gate.

This one satisfies the conditions for the unitary operator. Thus, it is obtained as $e^{-iJ_l\widehat{\sigma^x}\widehat{\sigma^x}t}$ = (CNOT)$_{12}$U3$_1$(CNOT)$_{12}$. This is shown in Fig. 9(a).

For **YY** operation:

Similarly, for $\widehat{\sigma_1^y}\widehat{\sigma_2^y}$ term,

A U3 gate is to be found. Among four types of U3 gates only the two shown below can be applied.

$$U3 = \begin{bmatrix} \cos\frac{\theta}{2} & \text{isin}\frac{\theta}{2} \\ \text{isin}\frac{\theta}{2} & \cos\frac{\theta}{2} \end{bmatrix}, \quad U3^\dagger = \begin{bmatrix} \cos\frac{\theta}{2} & -\text{isin}\frac{\theta}{2} \\ -\text{isin}\frac{\theta}{2} & \cos\frac{\theta}{2} \end{bmatrix} \quad (15)$$

Thus, $e^{-iJ_l\widehat{\sigma^y}\widehat{\sigma^y}t} = (CNOT)_{12}.U3_{21}.\ U3_{21}^\dagger.(CNOT)_{12}$

This is shown in Fig. 9(b).

For **ZZ** Operation,

Similarly, for $\widehat{\sigma_1^z}\widehat{\sigma_2^z}$ term,

Let us consider the Rz gate

$$Rz = \begin{bmatrix} e^{-i\frac{\theta}{2}} & 0 \\ 0 & e^{i\frac{\theta}{2}} \end{bmatrix} \quad (16)$$

This one satisfies the above conditions. While performing the calculations, it is observed that $e^{-iJ_l\widehat{\sigma^z}\widehat{\sigma^z}t}$ = (CNOT)$_{12}$Rz$_2$(CNOT)$_{12}$. This is shown in Fig. 9(c).

Thus, the circuit is completed for the Hamiltonian in general. Now, this calculation is extended for the Heisenberg model, XY model, transverse Ising model, longitudinal Ising model. The circuits for the four different models are shown in Fig 3.

4. Results

4.1. Initial State Preparation and unitary operation

The initial state is prepared by superposing the states of two qubits required to define the pairing Hamiltonian. This is done by putting a Hadamard gate on each qubit which provides contribution of all the qubits to the measurement. The unitary operators obtained in the previous section corresponding to the XX, YY, and ZZ type of interaction are then converted into quantum gates [19] and applied to form a circuit.

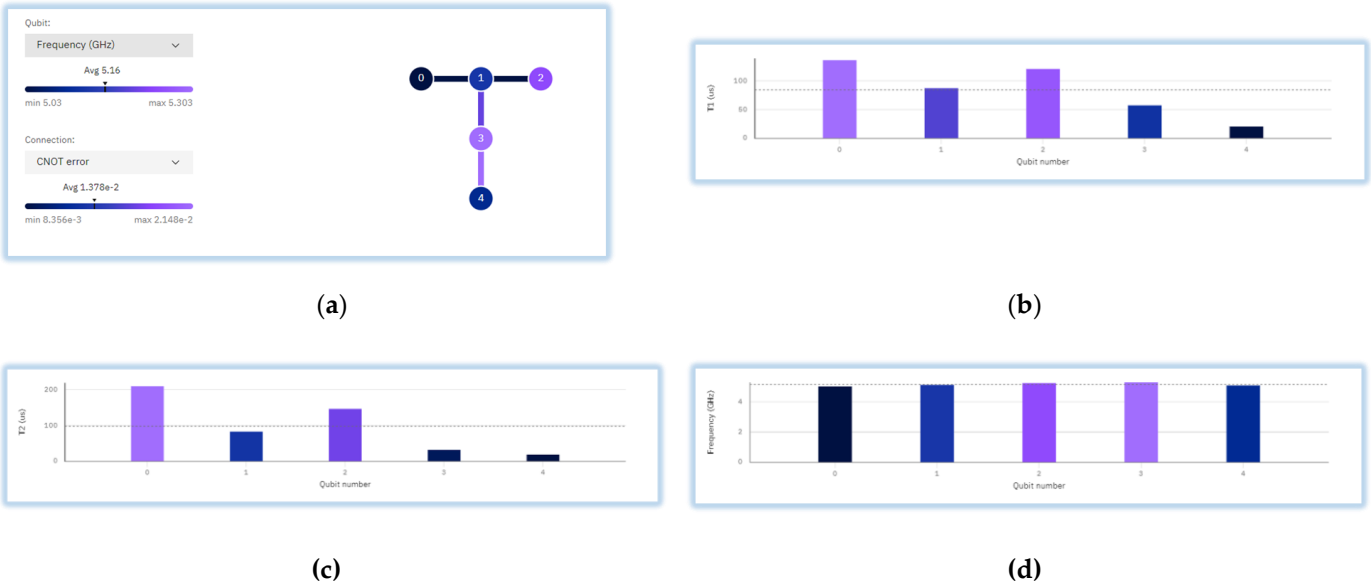

(a) **(b)**

(c) **(d)**

Figure 10. (a) Properties of the Quantum Processor used - (a) Map view of the IBMQ Lima quantum processor. (b) T1 (thermal relaxation time) of the qubits from qubit 0-4. (c) T2 (dephasing time) of the qubits from qubit 0-4. (d) Frequency of operation of the different number of qubits.

- For XX type of interaction: Comparing with the standard U3 gate (Eq. 15}) i.e, we find the parameters for the gate to be used as: $\theta = 2J_l t$, $\phi = -\pi/2$ and $\lambda = \pi/2$.
- For YY type of interaction: Parameters obtained for U3 gate: $\theta = 2J_l t$, $\phi = -\pi/2$ and $\lambda = \pi/2$. Parameters obtained for $U3^{\dagger}$ gate:$\theta = 2J_l t$, $\phi = \pi/2$ and $\lambda = -\pi/2$.
- For ZZ type of interaction: Comparing with the standard U1 gate, i.e.,

$$U1 = \begin{bmatrix} 1 & 0 \\ 0 & e^{i\lambda} \end{bmatrix} \quad (17)$$

$\lambda = 2J_l t$,

4.2. Quantum State Tomography for Suzuki-Trotter Decomposition of Quantum Circuit

In this section, Suzuki-Trotter decomposition is used to count the fidelity as a function of iterations of the quantum circuit. The circuit was iterated for n= 1,2,3,4,5,6,7,8,9,10. A Quantum state tomography [59] is used to get the theoretical and experimental density matrices, thus calculating the fidelity [60,61] of the circuit as shown in Eq. 18.

$$F(\rho,\sigma) = tr\sqrt{\sqrt{\rho}\ \sigma\sqrt{\rho}}$$

The general form of quantum state tomography is given by,

$$\rho = \frac{1}{2^N}\sum_{i=i_1,i_2,\ldots,i_N=0}^{2} T_{i_1,i_2,\ldots,i_N}\,\sigma_{i_1} \otimes \sigma_{i_2} \otimes \ldots \sigma_{i_N} \quad (19)$$

In particular, quantum state tomography reconstructs the density matrix of a quantum state by preparing the state many times and measuring them in a tomographically complete basis of measurement operators. In the paper, the circuit was measured with measurements of all qubits in each of the X, Y, and Z Pauli bases. For the 2-qubit system, these basis are II, IX, IY, IZ, XI, YI, ZI, XX, XY, XZ, YX, YY, YZ, ZX, ZY, ZZ. The probabilities of the states were taken by the experiment in the IBM real superconducting chip- IBMq Lima and the density matrix was constructed by using the formula as given in Eq. 19.

The experimental matrices of the circuits were computed through the density matrix as shown above. The experimental density matrix and the theoretical density matrix were compared and the fidelity of the quantum circuits were thus calculated. The whole circuit was simulated in 'IBMQ-Lima'.

It is of importance to know the parameters of the qubit system that is used in the experimental process. These parameters are shown in Fig. 10, which shows the map view of the qubits, T1(relaxation time) and T2(dephasing time) and the frequency of each qubit[62,63]. Here, the T1 (or longitudinal) relaxation process involves a loss of energy of the qubit. It's a relaxation from the excited to the ground state (hence longitudinal) and the corresponding timescale is the T1 time, while, the T2 (or transverse) relaxation time, or phase coherence time, describes how long the phase information of the superposition state of the qubit can be preserved for.

The Probabilistic simulations and calculations for the quantum systems are usually carried out using the Monte Carlo method on a classical computer [27]. Such methods were brought up to overcome the setback offered by exponentially growing phase spaces. Whereas, a quantum simulator [58] is usually very much under control of the experimenter. It is capable of simulating the dynamical behaviors of the physical models. Irrespective of the degree of internal correlations or entanglement between the degrees of freedom of the model, it can perform its job efficiently [57].

In this Section, the observations corresponding to the different circuits designed during quantum simulation of the Pairing Hamiltonian in superconductivity are explained. Fig.4,5,6,7 display the theoretical; and experimental density matrices, and the fidelity as a function of iteration for the Heisenberg model, XY, transverse Ising and longitudinal Ising model. The plots of experimental density matrix of 2 and 10 iterations are selected to be presented to choose the extremities of the iterations that have been conducted. It is to show how the density matrices is changing towards the theoretical density matrix as we are increasing the iteration. This increase in similarity to the theoretical density matrix as the iteration increases is a consequence of the Trotter decomposition.

It can be seen in Fig. 4., that for the Heisenberg model the experimental density matrix deviates clearly from the theoretical density matrix. There can be changes which can be seen in the experimental density matrix also as the number of iterations is increased. The fidelity thus found is seen to be oscillating till 10 iterations. This change corresponds to the increase in probability of a state as the iteration is increasing. This also takes a toll in the fidelity of the system as a whole. The error for every iteration is checked and a graph has been plotted to check the trend of variation. The variation of fidelity in the system shows the noise in the existing quantum processor. The average fidelity obtained for the system lies around 0.55 for the Heisenberg model. In Fig. 5, for XY model it was seen that the experimental density matrix changed as the iteration increased. This is again due to the change in probability of occurrence of each state at the certain iteration. As per the fidelity vs. iteration plot, the fidelity increased from 1 to 2 iteration, then decrease till 4 iterations. The fidelity then increases from 5 iteration till 7 iteration, decreasing at 8 iteration and again going high from 9 iteration and decreasing afterwards. The graph shows

the trend of the change. Variation of noise in the system may give such erratic results, though, an average value of the fidelity can be obtained to be within 0.5-0.55. For transverse Ising model (Fig. 6) it was noticed the experimental density matrix figures also changed for increasing iteration. The fidelity of the circuit increased from 1 iteration to 10 iteration but showing an erratic pattern. The average value of fidelity for this model can be found within 0.5-0.6. Lastly for longitudinal Ising model (Fig. 7) the experimental density matrix changed for increasing iteration from 2 to 10. The fidelity of the circuit followed the same pattern as the other Hamiltonian showing an erratic pattern. The average fidelity falls between the 0.4-0.55 for this model.

The variation of the fidelity shown for the four models can be accounted to the inclusion of noise from the real chip quantum computer. Noise parameter follows a periodic pattern which is affecting the fidelity of the circuits, thus showing a near periodic variation in the fidelity. Other than the noise parameter which certainly affects the fidelity, there are few more grounds which we can interpret from that. This is as per Trotter decomposition, as we are increasing the number of iterations, the fidelity of the circuit should increase. But, again in real experimental circuit inclusion of more number of gates as we are increasing the iteration would affect the fidelity so that it decreases. The fluctuations in the fidelity as we see is the effect of both of these parameters. It is also to be mentioned as the data points in the graph is low, thus we can see such fluctuations. But, if we increase the iterations to higher value and fit the graph, we would see that the fidelity would decrease and converge to zero.

In theory, if the number of gates increase in a circuit, due to inclusion of more noise, it is expected the fidelity to decrease. But, in experimental regime, this trend may be affected and can also give fidelity higher for systems with more gates, as seen in some models above.

Fig. 8 shows the variation of probability of possible states with respect to different values at $\theta = \frac{\pi}{2}$ and the time varies for t = 0,..,4. For Heisenberg Model, it is seen the state $|01\rangle$ is dominant at t = 0s which goes down to the lowest as t = 4s. For the XY model, the dominant state is $|01\rangle$ at time t = 0s and state $|00\rangle$ at t = 4s. For Transverse Ising Model, the dominant state at t=0s, the dominant state is $|00\rangle$ while at t= 4s, the dominant state is $|01\rangle$. For the Longitudinal Ising Model, the dominant state at t = 0s is $|00\rangle$ while at t= 4s, the dominant state is $|00\rangle$. The oscillatory behavior of the plots come from how time evolution operator works, ie., how the unitary operator changes in the states in the Bloch sphere.

5. Conclusions

This article includes algorithms and circuits for simulating the pairing Hamiltonians based on various nearest-neighbor interactions, e.g., Heisenberg Hamiltonian, longitudinal Ising Hamiltonian, XY Hamiltonian and transverse Ising Hamiltonian, which are available in the solid-state quantum devices. The Hamiltonians are all been implemented on IBM superconducting qubit quantum computer. It was found out the Quantum State Tomography for the different Hamiltonian thus finding the fidelity vs. iterations of the different circuits using Suzuki-Trotter decomposition. The experimental density matrix has been seen to steadily approach the theoretical density matrix as the iteration is increased. This opens up how exotic physics problems can be tackled by transforming the Hamiltonians of such models in quantum circuits and simulating them in Quantum Computers. Quantum State Tomography proves to be an advantageous method to find the density matrices of such models with which if the iteration is increased by Trotter decomposition, the experimental results on quantum chips would perfectly follow the theoretical result. The fidelity vs. iteration served as a metric to see how the experimental matrix is changing as the iteration is increased. The variation of the fidelity implies the noise

parameter in the quantum system which is an inherent phenomenon in the "Noisy intermediate scale quantum (NISQ)" era.

6. Acknowledgement

The authors acknowledge the support of IBM Quantum Experience for providing the access of quantum processors. The views expressed are those of the authors and do not reflect the official policy or position of IBM or IBM Quantum Experience team.

References

1. A. Smith, M. S. Kim, F. Pollmann, et al. Simulating quantum many-body dynamics on a current digital quantum computer. npj Quantum Inf 5, 106 (2019)
2. S. G. Schirmer, I. C. H. Pullen, A. I. Solomon Controllability of Quantum Systems IFAC Proceedings Volume 36, Issue 2, (2003)
3. S. Lloyd, Universal quantum simulators, Science 273, 1073-1078 (1996)
4. A. Shabani, M. Mohseni, S. Lloyd, R. L. Kosut, and H. Rabitz Estimation of many-body quantum Hamiltonians via compressive sensing Phys. Rev. A 84, 012107 (2011)
5. C W. Bauer, Wibe A. de Jong, B. Nachman, D. Provasoli A quantum algorithm for high energy physics simulations Phys. Rev. Lett. 126, 062001 (2021)
6. Dawei Lu, Boruo Xu, Nanyang Xu, Zhaokai Li, Hong- wei Chen, Xinhua Peng, Ruixue Xua and Jiangfeng Du, Quantum chemistry simulation on quantum computers: theories and experiments Phys. Chem. Chem. Phys.,14, 9411-9420 (2012)
7. C. Langer, High Fidelity Quantum Information Processing with Trapped Ions. (2006)
8. L. Cohen, A. J. Brady, Z. Huang, H. Liu, D. Qu, J. P. Dowling, and M. Han Phys. Rev. Lett. 126, 020501 (2021)
9. M. Saffman, Quantum computing with neutral atoms, National Science Review, Volume 6, Issue 1, Pages 24–25 (2019)
10. V. Salari, H. Naeij A. Shafiee, Quantum Interference and Selectivity through Biological Ion Channels. Sci Rep 7, 41625 (2017)
11. D. DeMille, Quantum Computation with Trapped Polar Molecules. Phys. Rev. Lett. 88. 067901. (2002)
12. X.-F. Shi, Rydberg quantum computation with nuclear spins in two-electron neutral atoms, Frontiers of Physics, vol. 16, no. 5, Apr. 2021
13. G. Milburn, Photons as qubits. Physica Scripta. 014003 2009
14. R. Blatt, C. Roos, Quantum simulations with trapped ions. Nature Phys 8, 277–284 (2012)
15. I.M. Georgescu, S. Ashhab, and Franco Nori Rev. Mod. Phys. 86, 153 (2014)
16. Ma, H., Govoni, M. , Galli, G. Quantum simulations of materials on near-term quantum computers. npj Comput Mater 6, 85 (2020)
17. Faroukh, Yousuf. Quantum Computers Vs Conventional Computers: A Study on the Larger Scale. (2018)
18. M. A. Nielsen and I. L. Chuang, quantum Computation and Quantum Info.: 10th Anni. Ed, Cambridge Univer- sity Press40 W. 20 St. New York, NYUnited States, 708 (2011)
19. Z. Wang, X. Gu, L. A. Wu, and Y. x. Liu, Quantum simulation of pairing hamiltonians with nearest-neighbor interacting qubits, Phys. Rev. A 93, 062301 (2016)
20. R. Babbush, D. W. Berry,J. R. McClean, et al. Quantum simulation of chemistry with sublinear scaling in basis size. npj Quantum Inf 5, 92 (2019)
21. C. Outeiral, M. Strahm, J. Shi, Garr M. Morris, Simon C. Benjamin, C. M. Deane, WIREs Comp. Mol. Science, (2020)
22. J. Bardeen, L. N. Cooper, and J. R. Schrieffer Phys. Rev. 108, 1175
23. Y. Alhassid, K. N. Nesterov Mesoscopic superconductivity in ultrasmall metallic grains AIP Conf. Proc. 1619, 24 (2014)
24. X. D. Yang, A. M. Wang, F. Xu, and J. Du, Experimental simulation of a pairing Hamiltonian on an NMR quantum computer, Chem. Phys. Lett. 422, 20-24 (2006)
25. A. Di Paolo, T. E. Baker, A. Foley, et al. Efficient modeling of superconducting quantum circuits with tensor networks. npj Quantum Inf 7, 11 (2021)
26. Z. I. Alferov, The history and future of semiconductor heterostructures. Semiconductors 32, 1–14 (1998)
27. G. Ortiz, J. E. Gubernatis, E. Knille, and R. Laflamme, Quantum algorithms for fermionic simulations, Phys. Rev. A 64, 022319 (2001)
28. R.P. Feynman, Simulating physics with computers. Int J Theor Phys 21, 467–488 (1982)
29. A. Pathak, Elements of Quantum Computation and Quantum Communication, (2013)
30. Wikipedia, Quantum logic gate, https://en. wikipedia.org/wiki/Quantum_logic_gate Accessed on February 2019
31. M. Georgescu, S. Ashhab, and F. Nori. Quantum Sim- ulation, Rev. Mod. Phys. 86, 153-185 (2014)
32. Pedersen, Line Hjortshoj and Moller, Niels Mar- tin and Molmer, Klaus. Fidelity of quantum operations. DOI=10.1016/j.physleta.2007.02.069
33. M. H. Devoret, R. J. Schoelkopf. Superconducting cir- cuits for quantum information: an outlook. Science. (2013)
34. J. Clarke,F.K. Wilhelm. Superconducting quantum bits. Nature. (2008)
35. J. Q. You and F. Nori, Phys. Today 58(11), 42 (2005)
36. L. A. Wu, M. S. Byrd and D. A. Lidar, Phys. Rev. Lett. 89, 057904 (2002)

37. T. P. Orlando, J. E. Mooij, L. Tian, C. H. van der Wal, L. S. Levitov, S. Lloyd, and J.J. Mazo, Phys. Rev. B 60, 15398 (1999)
38. J. Q. You, J. S. Tsai, and F. Nori, Phys. Rev. Lett. 89, 197902 (2002)
39. S. Gangopadhyay, Manabputra, B. K. Behera, P. K. Panigrahi, Generalization and demonstration of an entanglement-based Deutsch-Jozsa-like algorithm using a 5-qubit quantum computer, Quantum Inf. Process. 17, 160 (2018)
40. A. Mandviwalla, K. Ohshiro and B. Ji, "Implementing Grover's Algorithm on the IBM Quantum Computers," 2018 IEEE International Conference on Big Data (Big Data), Seattle, WA, USA, 2018, pp. 2531-2537
41. J. Stenger, N. Bronn, D. Egger, D. Pekker. (2020). Simulating the dynamics of braiding of Majorana zero modes using an IBM quantum computer.
42. I. M. Georgescu, S. Ashhab, and Franco Nori Rev. Mod. Phys. 86, 153
43. M. Cattaneo, M. A.C. Rossi, G.García-Pérez, R. Zambrini, S. Maniscalco PRX Quantum 4, 010324 (2023)
44. K. Sarkar, B. K. Behera, and P. K. Panigrahi, A robust tripartite quantum key distribution using mutually share Bell states and classical has values using a complete graph network architecture, DOI: 10.13140/RG.2.2.27559.39844 (2019)
45. R. Agarwal, C. K. Sethi, N. K. Gupta, and P. K. Panigrahi, Comparison of advantages in quantum teleportation using cluster state and coined quantum walks, DOI: 10.13140/RG.2.2.35192.80648 (2020)
46. A. Warke, B. K. Behera, and P. K. Panigrahi, Experimental Realization of Three Quantum Key Distribution Protocols, DOI: 10.13140/RG.2.2.15812.78725 (2019)
47. R. Saini, A. Papneja, B. K. Behera, and P. K. Panigrahi, Experimental Realization of Differential Phase Shift Quantum Key Distribution on IBM QX, DOI: 10.13140/RG.2.2.10904.14089 (2019)
48. B. K. Behera, A. Banerjee, P. K. Panigrahi, Experimental realization of quantum cheque using a five-qubit quantum computer, Quantum Inf. Process. 16, 12 (2017)
49. B. K. Behera, T. Reza, A. Gupta, and P. K. Panigrahi, Designing Quantum Router in IBM Quantum Computer, Quantum Inf. Process. 18, 328 (2019)
50. B. K. Behera, S. Seth, A. Das, and P. K. Panigrahi, Demonstration of Entanglement Purification and Swap- ping Protocol to Design Quantum Repeater in IBM Quantum Computer, Quantum Inf. Process. 18, 108 (2019)
51. R. McDermott, R. W. Simmonds, Matthias Steffen, K. B. Cooper, K. Cicak, K. D. Osborn, Seongshik Oh, D. P. Pappas, John M. Martinis, Science 307, 1299 (2005)
52. D. Loss and D. P. DiVincenzo Phys. Rev. A 57, 120
53. D. W. Leung, Isaac L. Chuang, F. Yamaguchi, and Y. Yamamoto Phys. Rev. A 61, 042310
54. A. Houck, H. T¨ureci and J. Koch, On-chip quantum simulation with superconducting circuits. Nature Phys 8, 292–299 (2012)
55. D. J. Griffith, Quantum Mechanics.
56. R. Barends, J. Kelly, A. Megrant , A. Veitia, D. Sank, E. Jeffrey, T. C. White, J. Mutus, A. G. Fowler , B. Campbell, Y. Chen , Z. Chen, B. Chiaro , A. Dunsworth, C. Neill, P.O'Malley , P. Roushan, A. Vainsencher, J. Wenner , A. N. Korotkov , A. N. Cleland, J. M. Martinis, Superconducting quantum circuits at the surface code threshold for fault tolerance. Nature. ;508 (7497):500-3. (2014)
57. F. Tacchino, A. Chiesa, S. Carretta, and D. Gerace, Quantum computers as universal quantum simulators: state of art and perspectives, Advanced Quantum Technologies 3, 1900052 (2020)
58. J. T. Barreirro, M. Mueller, P. Schindler, M. Hennrich, C. F. Roos, P. Zoller, and R. Blatt, An open system quantum simulator with trapped ions, Nature 470, 486–491
59. Altepeter, J.B., James, D.F., Kwiat, P.G. 4 Qubit Quantum State Tomography. In: Paris, M., Řeháček, J. (eds) Quantum State Estimation. Lecture Notes in Physics, vol 649. Springer, Berlin, Heidelberg.
60. Jozsa R. Fidelity for Mixed Quantum States. Journal of Modern Optics. 1994;2315 - 2324.
61. A. Uhlmann, The "transition probability" in the state space of a ∗-algebra, Reports on Mathematical Physics, Volume 9, Issue 2, 1976
62. Carroll, M., Rosenblatt, S., Jurcevic, P. et al. Dynamics of superconducting qubit relaxation times. npj Quantum Inf 8, 132 (2022).
63. Choi, Y., Joynt, R. Anisotropy with respect to the applied magnetic field of spin qubit decoherence times. *npj Quantum Inf* **8**, 70 (2022).